This is the peer-reviewed version of the article:

Formation kinetics and cation inversion in mechanically activated $MgAl_2O_4$ spinel ceramics

Nina Obradović[1,*], William G. Fahrenholtz[2], Suzana Filipović[1], Smilja Marković[1],

Vladimir Blagojević[1], Steva Lević[3], Slobodan Savić[4], Antonije Đorđević[4,5], Vladimir Pavlović[1]

[1]Institute of Technical Sciences of the Serbian Academy of Sciences and Arts,

11000 Belgrade, Serbia

[2]Materials Science and Engineering, Missouri University of Science and Technology,

Rolla, Missouri, United States

[3]Faculty of Agriculture, University of Belgrade, 11081 Belgrade, Serbia

[4]School of Electrical Engineering, University of Belgrade, 11000 Belgrade, Serbia

[5]Serbian Academy of Sciences and Arts, 11000 Belgrade, Serbia

Abstract

Solid-state mechanical activation of MgO and α-Al_2O_3 powders was used to produce

$MgAl_2O_4$. The cation site occupancy in the resulting $MgAl_2O_4$ spinel was investigated using

different methods. Differential thermal analysis and thermal gravimetry showed that

mechanical activation reduced the spinel formation temperature by around 200 ^oC, and the

corresponding activation energy by about 25 %. In addition, characteristic temperatures for

evaporation of physisorbed water and decomposition of $Mg(OH)_2$ shifted to lower values, and

* Corresponding author: nina.obradovic@itn.sanu.ac.rs (Dr. Nina Obradović)

peaks were more pronounced. Raman spectra were used to characterize the degree of inversion as a function of the sintering temperature for all of the sintered specimens, indicating that the breaking point for ordering of the crystal structure was around 1500 $^{\circ}$C for non-activated samples, and 1400 $^{\circ}$C for activated samples.

Key words: mechanical activation; DTA; Raman spectroscopy; sintering kinetics; spinel.

Introduction

Spinel ($MgAl_2O_4$) is the only compound in the $MgO-Al_2O_3$ binary system [1]. It is a material of great interest owing to its high melting point (> 2100 $^{\circ}$C), excellent mechanical, thermal, and chemical properties, and low dielectric constant (~ 8), that make it particularly useful in high-temperature applications [2]. $MgAl_2O_4$ can be synthesized through direct solid-state reaction [3, 4], ultrasonic treatment [5], gel casting [6], wet chemical solution techniques [7, 8], co-precipitation [9], and mechanical activation [10, 11].

Mechanical activation (MA) is a complex physico-chemical process, which increases the chemical activity and potential energy of the treated material, causing changes in the specific surface area and internal energy, and generally increasing the free energy of the system [12]. During MA, attrition reduces the crystallite size of the material, which can lead to deformation or changes in the crystal structure, accompanied by generation of defects [13–16]. The influence of the mechanical forces on the material during grinding leads to elastic and plastic deformation, which change the physico-chemical properties of the material [17]. The reactivity of solid materials increases as a result of the structural changes, due to generation of

2

point defects (vacancies, interstitial atoms, and impurity atoms), line defects (atom aggregations on the crystal surface), volume defects (pores and impurities), and electronic defects (electrons and holes) [18, 19]. These changes indicate that the mechanical energy was transformed into crystal lattice defects, leading to fragmentation, a decrease in the particle size, and changes in the surface area and the physico-chemical properties of crushed material. MA is commonly used as a pre-sintering process to improve the reactivity of the system, lower the temperature and time required for densification or amorphizing the system [20–22].

Spinels exhibit varying degrees of inversion, or disorder among occupancy of A and B sites by the A and B cations, presented in Figure 1. The general formula of spinel type of compounds is AB_2O_4, where A is divalent and B is trivalent. For normal spinels, the A cations occupy 8 of the 64 tetrahedral sites, and B cation occupy half of the octahedral sites [23, 24]. With increased temperature or pressure, exchange occurs between Mg and Al cations, leading to the formation of a partially inverted spinel. Inversion usually occurs in the temperature range of 800 to 1000 ºC [25].
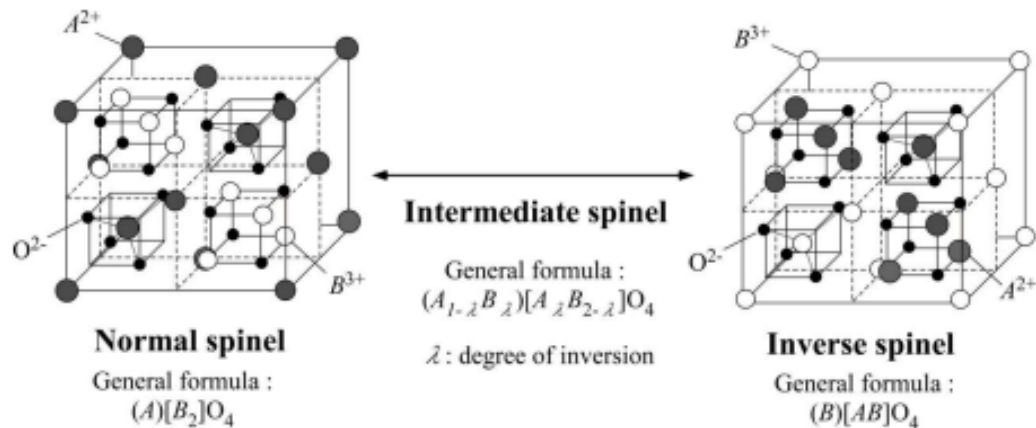

Figure 1 Scheme of normal and inverse spinel crystal struicture.

3

Raman spectroscopy can be used to examine the degree of inversion in spinel compounds. To the best of our knowledge, no Raman studies have been reported for spinel specimens sintered above 1400 °C, or for the influence of MA on inversion investigated by characterizing Raman modes. The aim of this study is to determine the influence of the mechanical activation on the microstructure, and spinel formation kinetics, which is examined in detail by DTA–TG analysis, as well as the influence of MA on the site occupancy in the $MgAl_2O_4$ spinel, followed by Raman spectroscopy.

Experimental procedure

Initial powders were a mixture of high-purity MgO and α-Al_2O_3 (all 99.9 % purity Sigma–Aldrich, p.a.), in a 1:1 molar ratio to produce stoichiometric $MgAl_2O_4$. The powders were mixed by ball milling to homogenize them without significant particle size reduction. The samples underwent mechanical activation for 60 min in a high-energy planetary ball mill (Planetary Ball Mill Retsch PM 100), in air, using Y-stabilized ZrO_2 vials and balls (5 mm in diameter). The ball-to-powder weight ratio was 40:1 with a rotation speed of 400 rpm. Powders were sieved after milling. The resulting powders were labelled based on the activation time as AM–0 and AM–60. The binder-free powders were compacted at 300 MPa using a uniaxial double action pressing process with an 8 mm diameter tool (hydraulic press RING, P-14, VEB THURINGER). Compacts were placed in an Al_2O_3 boat and heated in a tube furnace (Lenton Thermal Design Typ 1600). Conventional sintering was performed in air, at temperatures from 1200 to 1600 °C, with heating rates of 10 °C·min^{-1} and 2 h dwell time (isothermal regime on the maximum achieved sintering temperatures). The bulk densities were calculated measured

4

mass, diameter, and thickness of the sintered specimens. Specimens were labelled according to the sintering temperature, where AM–60–1200 represents the sample mechanically activated for 60 min and sintered at 1200 °C, etc. The theoretical density (TD) of $MgAl_2O_4$ was assumed to be 3.60 g·cm^{-3} based on previous reports [23].

Thermal behavior of powders was determined by simultaneous thermal gravimetry and differential thermal analysis (TG–DTA) (Setsys, SETARAM Instrumentation, Caluire, France) from 25 to 1500 °C under the air flow of 20 ml·min^{-1}, in an Al_2O_3 pan, at heating rates of 10, 20, and 30 °C·min^{-1}. Peak deconvolution and kinetic analyses were performed using ThermV v0.2 software package [26]. The degree of conversion (α) was calculated for each peak as the ratio of the partial peak area at a given temperature to the area of the entire peak.

The morphology of the powders and sintered specimens was analyzed by the scanning electron microscopy (SEM) (JEOL JSM-6390 LV). Prior to SEM observations, the powders and crushed sintered samples were coated with Au to minimize charging.

The XRD patterns for pulverized sintered specimens were collected on an Ital Structure APD 2000 X-ray powder diffractometer using CuKα radiation (λ = 1.5418 Å) in a range 2θ = (20 – 80 °) with a step-width of 0.02 ° and a constant counting time of 1 s per step.

Raman spectra were recorded in the 200–900 cm^{-1} range using a XploRA Raman spectrometer from Horiba Jobin Yvon, with a 532 nm laser at a maximum output power of 20–25 mW. To prevent damage by the laser, power was reduced using a 10 % filter. All measurements were realized using a spectrometer equipped with a 2400 lines mm^{-1} grating, with 10 s/5 cycles acquisition time. A microscope objective (50×, long working distance) was used for laser focusing.

An Agilent E5061A network analyzer was used to measure the relative dielectric permittivity (dielectric constant) and the loss tangent of the sintered specimens in the frequency range between 10 MHz and 3 GHz, in a coaxial test chamber. The reflection coefficient of the chamber was measured by the analyzer and electromagnetic models were used to extract the relative complex permittivity of the specimens.

Results and discussion

Scanning electron micrographs of the starting powders are presented in Figure 2. The non-activated powder consisted of two different types of particles: 1) smaller primary particles approximately 300 nm in diameter that was present in agglomerates around 1 µm in size; and 2) larger, polygonal particles, ranging in size from about 1.5 µm to 2.5 µm.
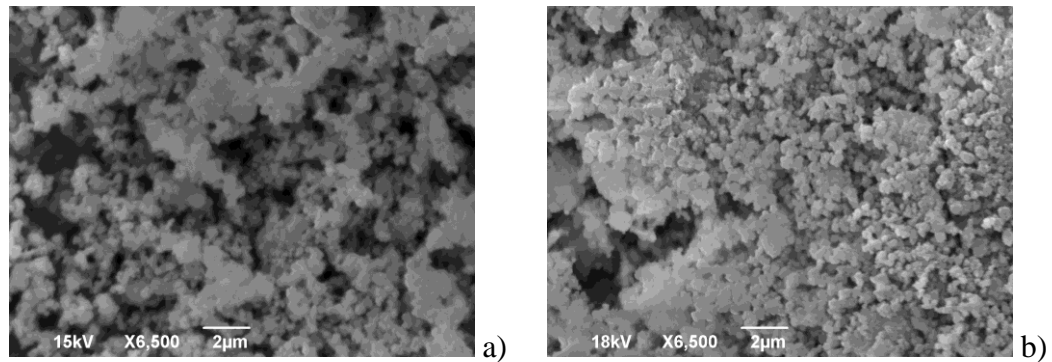

Figure 2 SEM micrographs of: a) non-activated and b) 60 min activated powder.

The influence of MA on powder morphology is evident in the powder activated for 60 min, which appeared to be more homogeneous with an obvious reduction in agglomerate

6

and particle size. The change in morphology indicated that smaller particles formed as MgO agglomerates were comminuted. Larger alumina particles were also broken down into particles that were 1 μm or smaller in diameter.

<mark>The DTA curves of non-activated powders had some very weak peaks shown in Figure 3. In contrast, the activated samples had more pronounced peaks as shown in Figure 4.</mark> In both non-activated and activated powders, an increase in heating rate led to more pronounced endothermic peaks. All curves possessed an endothermic peak at around 100 °C, which was attributed to loss of adsorbed water. In the temperature range of 200–350 °C several processes occurred, such as loss of chemically bound water or related compounds [27, 28]. Given that both the mechanical activation and thermal experiments were performed in the air, it is likely that carbon-dioxide was physisorbed or chemisorbed in the activated powders, leading to additional desorption processes at higher temperatures.
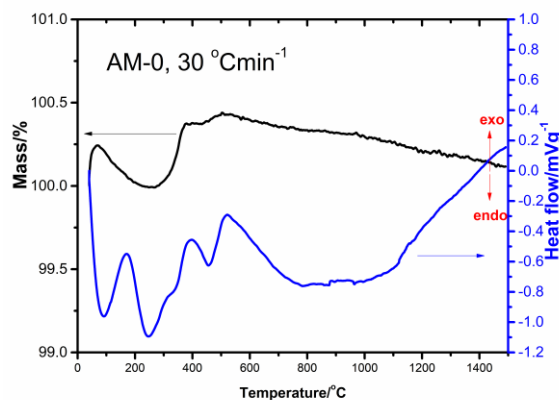

7
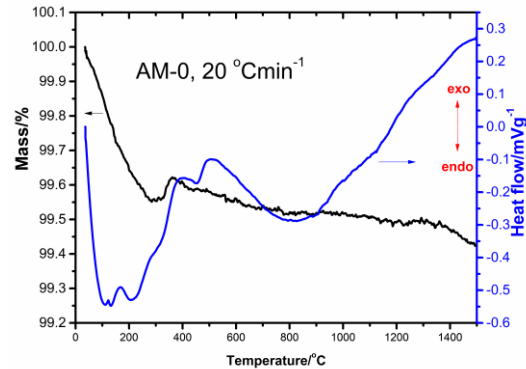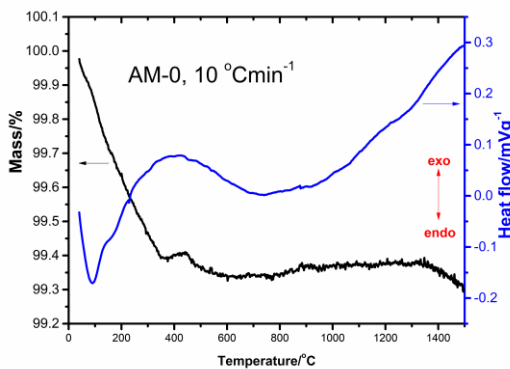
Figure 3 DTA–TG results for non-activated samples with different heating rates.

Significantly higher mass loss was observed for mechanically activated samples. The higher mass losses further reinforces the assignments of mass loss to loss of water and/or CO_2, with mass losses of 0.4–0.6 wt. % in non-activated and 3.5–4 wt. % in activated samples. Around 455 °C, an endothermic peak was observed for all samples, which can be attributed to dehydration of magnesium hydroxide and decomposition of magnesium carbonate, [29, 30]. Unlike other peaks, the peak due to dehydration of magnesium hydroxide and carbonate decomposition was more pronounced in non-activated samples, which is consistent with the fact that the mechanical activation in air would partially disrupt the existing surface layer due to the increase in surface area while also introducing a significant amount of additional carbon dioxide into the powder mixture prior to thermal analysis. Above 500 °C, no additional mass changes were observed. At temperatures above 500 °C, a relatively small endothermic peak was observed around 700 °C for mechanically activated samples.
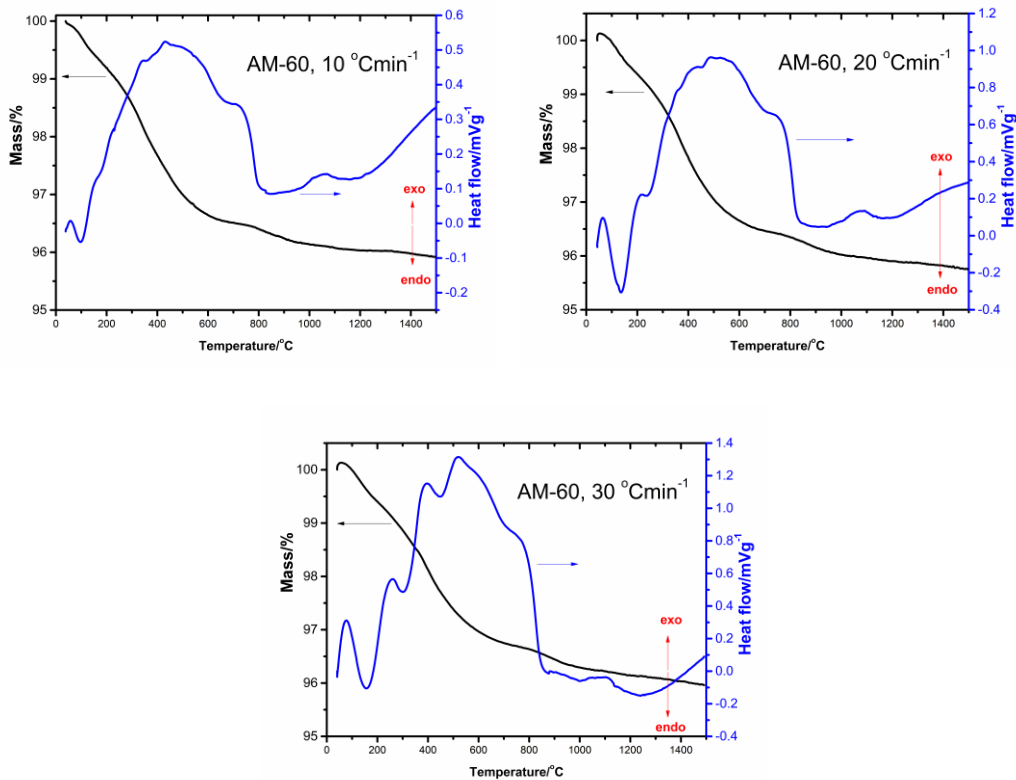
8

Figure 4 DTA–TG results for activated samples with different heating rates.

Mechanical activation led to more rapid spinel formation at lower temperatures. An exothermic peak was observed for all samples in the temperature range of 950–1400 $^{\circ}$C, which corresponded to spinel formation [9] (Figure 5). The lower temperature of the exothermic peak in the activated samples indicated significantly greater reactivity of the powder activated for 60 min. Furthermore, the reaction required less energy to reach completion based on the overall activation energies (E_a), calculated using Kissinger method [31]. The E_a values were 580±10 kJ·mol^{-1} for the non-activated powder and 420±15 kJ·mol^{-1} for the activated sample. The non-activated powder had a similar E_a to a previously reported values of around 550 kJ·mol^{-1} [32]. The corresponding values of the pre-exponential factor (A) were also lower for the activated powders with lnA values of 31.0±0.5 for the non-activated powder and

9

22.0±0.8 for the activated powder. The lower value of the activation energy for spinel formation from mechanically activated powders is consistent with the reduction in observed spinel formation temperature from 1100–1400 °C for the non-activated powder to 950–1150 °C for the activated powder.
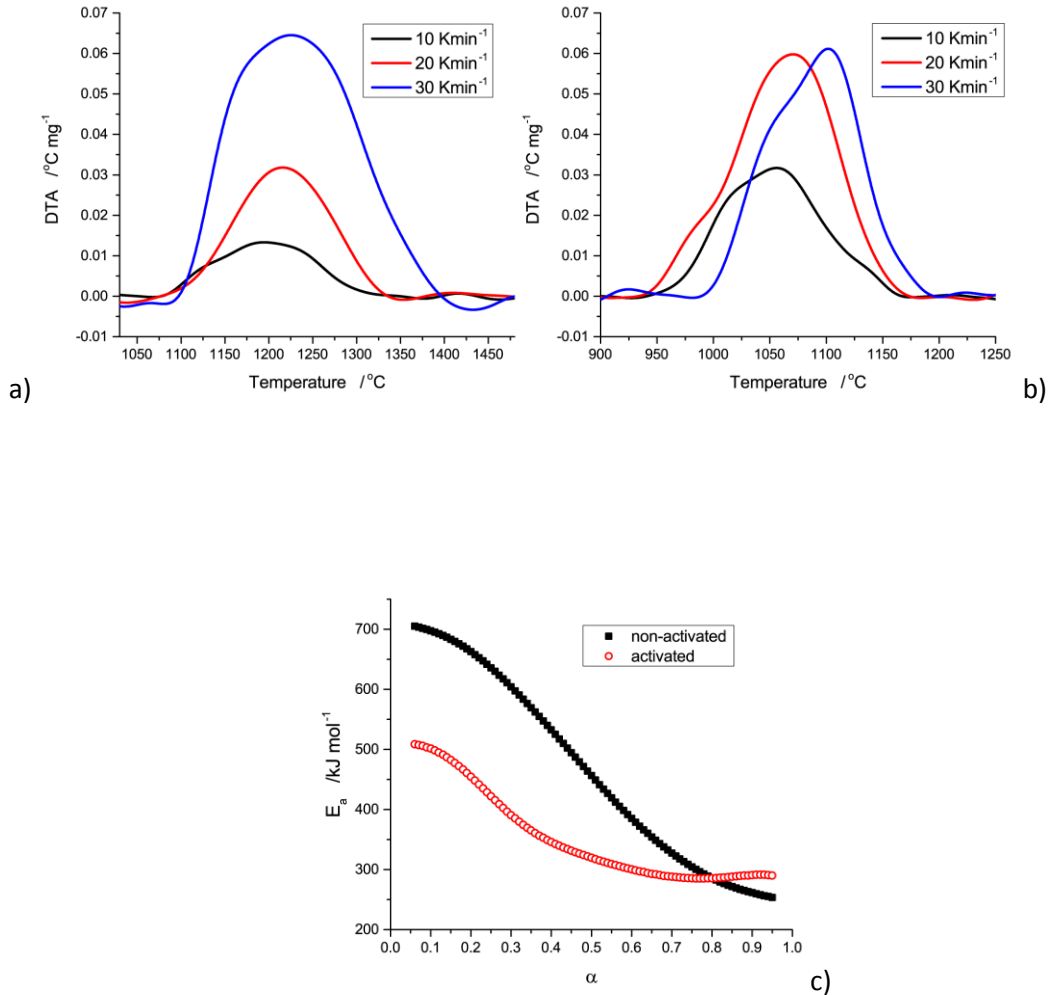

a)

b)

c)

Figure 5 Spinel formation peaks from DTA in: a) non-activated and b) activated powders;

c) Effective values of E_a (isoconversional Ortega method) for formation of spinel.

10

The reduction in formation temperature can be attributed to the increase in the powder surface area, which increases the number of potential nucleation sites for spinel formation in the mechanically activated precursor powders and increases the concentration of defects caused by the mechanical activation [13]. The peaks in mechanically activated powders were also considerably narrower, indicating faster reaction for activated powders. Based on this analysis, mechanical activation reduces the spinel formation temperature and increases the reaction rate by reducing the activation energy required for reaction. Figure 5 also shows the effective apparent values of the activation energy for both non-activated and activated samples, obtained using the isoconversional Ortega method [33] for the exothermic spinel formation peak. Calculated values of E_a are considerably lower for mechanically activated samples, and the shape of both curves, with a downward slope, indicates a process complicated by diffusion [34], consistent with mass transport during formation of spinel in the solid state.

Figure 6 shows comparison of simulated curves calculated using kinetic parameters obtained from Kissinger method above and assuming D2: 2-D diffusion reaction model [35]. These show that non-activated samples exhibit, in general, higher agreement with D2 model, while mechanically activated samples only show good agreement in the initial stage of the reaction, which can be attributed to the increased complexity caused by the mechanical activation. General agreement with 2-D diffusion reaction model can be expected for a solid-state reaction in the powder mixture.
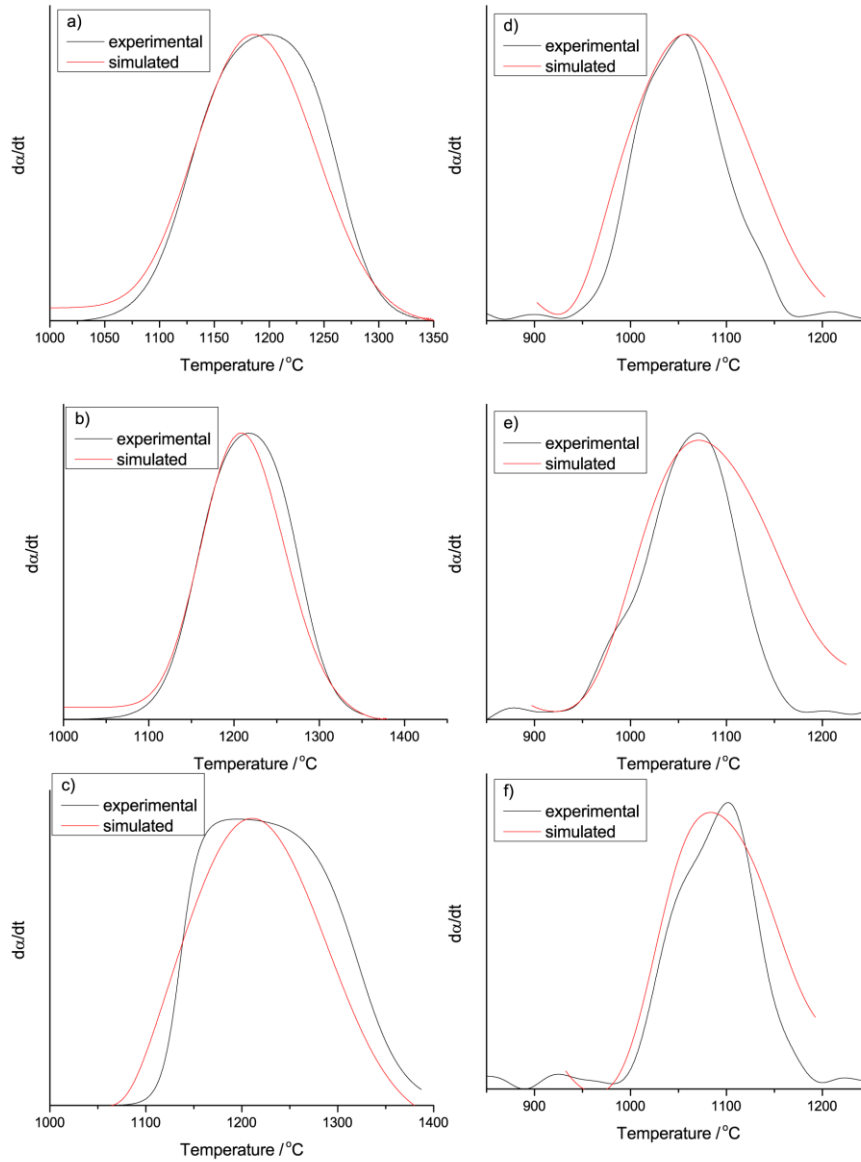
11

Figure 6 Comparison of experimental and simulated curves for non-activated (a-c) and activated (d-f) samples at different heating rates with presumed model D2.

Scanning electron micrographs of fracture surfaces of the sintered specimens produced from the non-activated powders (AM–0 series) are presented in Figure 7. The non-activated specimen sintered at 1200 ºC for 2 h consisted of particles approx. 500 nm in size with necks that formed during sintering. Specimen AM–0–1300 showed a higher degree of sintering. In

addition to the non-uniform grain size, cracks were present, which were presumed to form around regions that corresponded to agglomerates in the initial powder compact that had higher density after sintering at this temperature. After sintering at 1400 ^{o}C, the observed microstructure was very similar to the samples sintered at lower temperatures, with breakage between grains, irregular pores, and agglomerates visible, indicating that the grain growth had not yet started and that this specimen remained in the intermediate stage of sintering.
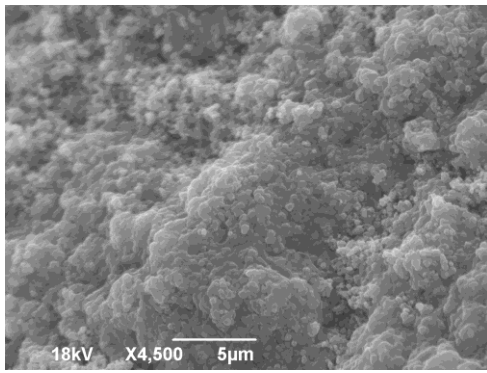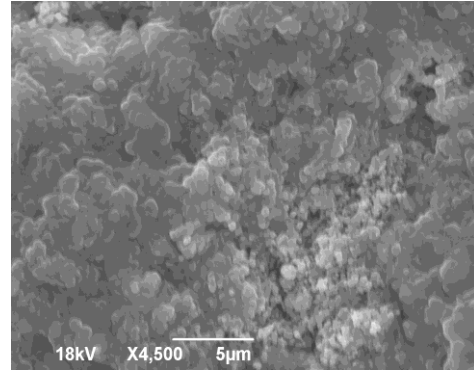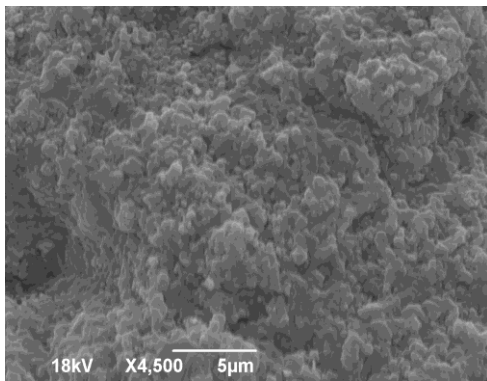
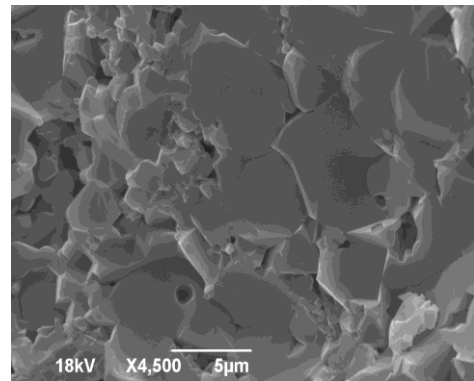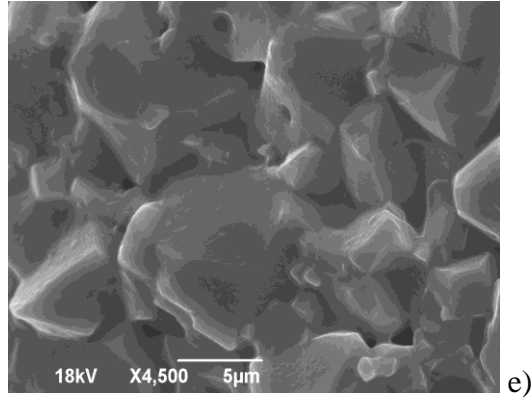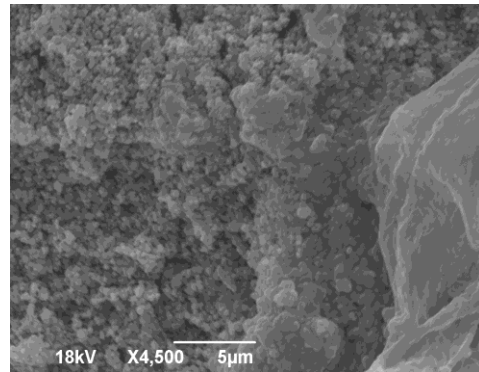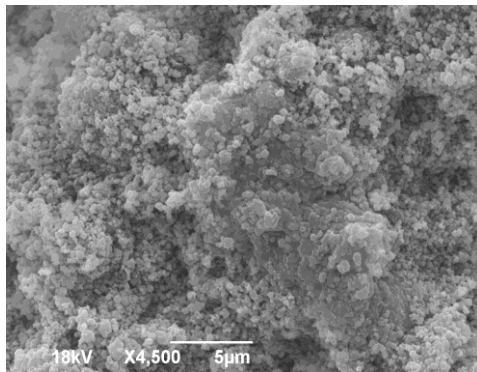**Figure 7** SEM micrographs of fracture surfaces of specimens: a) AM–0–1200, b) AM–0–1300, c) AM–0–1400, d) AM–0–1500, and e) AM–0–1600.

Spherical pores and breakage through grains observed for AM–0–1500 indicated that this specimen had entered the final sintering stage. Some breakage between smaller grains was observed, confirming that those grains were not fully developed, with non-uniform grain growth observed, as well. When the sintering temperature was increased to 1600 °C, all of the grains were polygonal with small, spherical, and closed pores. Based on its appearance, AM–0–1600 had a high relative density and appeared to be completely sintered, in agreement with measured densities (see Table 1).
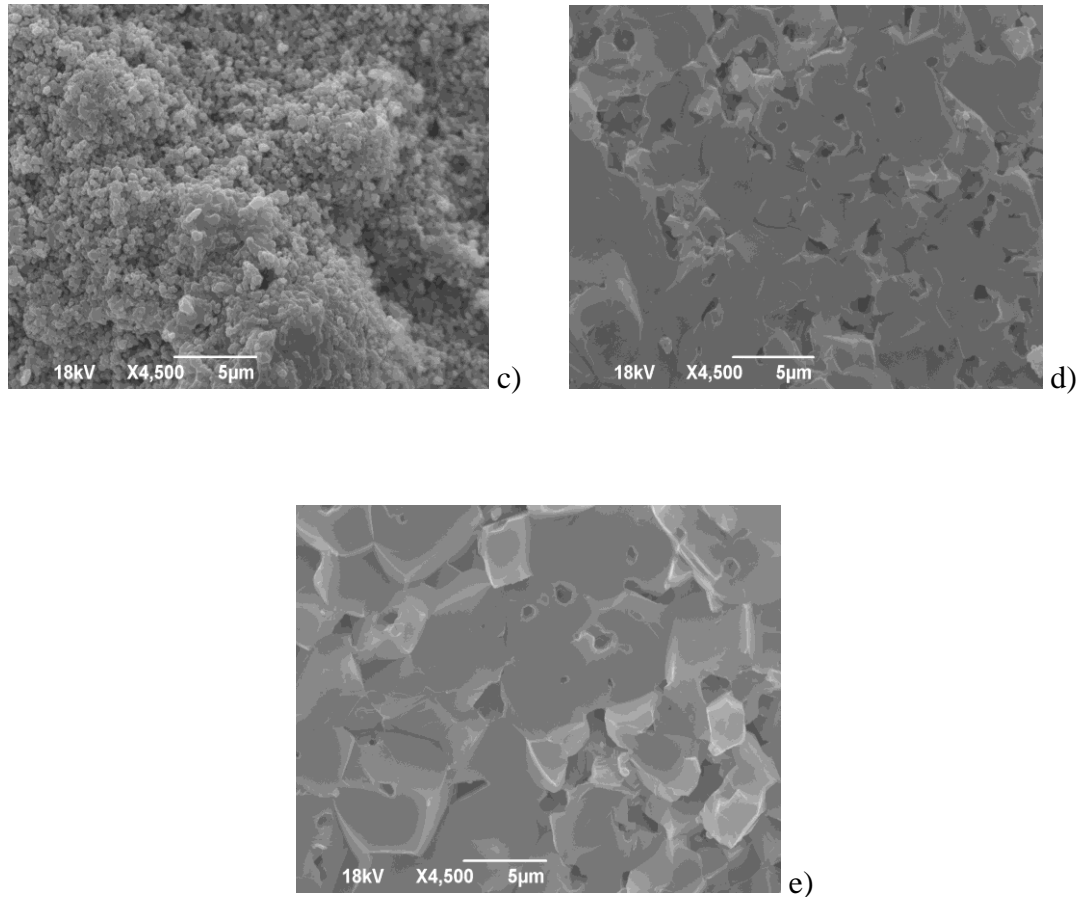

a)

b)

Figure 8 SEM micrographs of fracture surfaces of sintered samples: a) AM–60–1200,

b) AM–60–1300, c) AM–60–1400, d) AM–60–1500, and e) AM–60–1600.

Figure 8a shows that AM–60–1200 consisted of powder particles less than 500 nm in size, with fully open porosity and contact necks formed between all of the particles. The AM–60–1300 specimen had some regions that appeared to be sintered to a higher relative density (see the right part of Figure 8b), with the other portion of the sample indicating that the specimen consisted of particles which had started to form necks. The presence of the open porosity and non-uniform microstructural regions indicated that this specimen was still in the initial sintering stage. The main characteristics for AM–60–1400 were breakage through grains

and uniform grain size with open porosity, where the pores were becoming more spheroidal and the dominant fracture mode was through grain. At this temperature, microstructures were almost completely compact. Non-uniform grain growth was observed in AM–60–1500 with uneven pores. Compared to lower sintering temperatures, the degree of porosity was significantly lower and additional polygonal grains had formed. Most pores were coalescing into closed pores, indicative of final stage sintering, which was observed in AM–60–1600.

The XRD patterns of sintered specimens are presented in Figure 9. All reflections were identified using the corresponding JCPDS card 33–0853 for $MgAl_2O_4$. All peaks were sharp, indicating that the MgO and Al_2O_3 powders reacted to form the spinel phase of $MgAl_2O_4$.
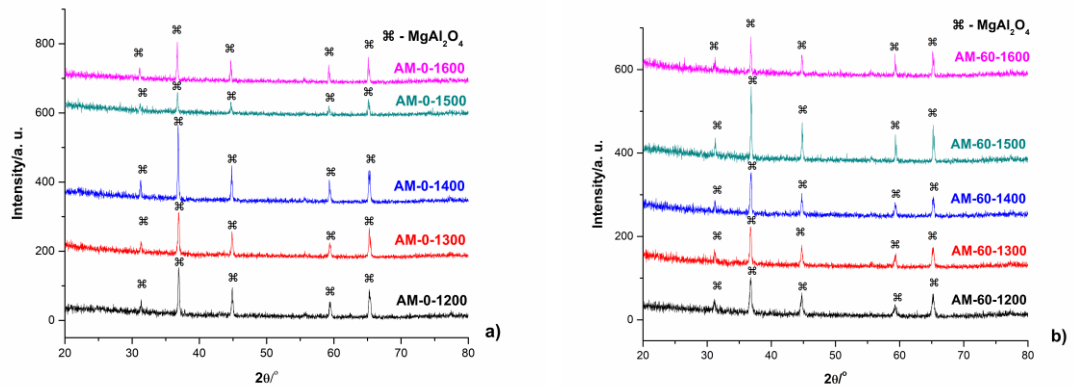
Figure 9 XRD patterns of: a) non-activated powder (AM–0) and b) powder activated for 60 minutes (AM–60), after heating to various temperatures for 2 h in air [10].

The relative permittivity ($\boldsymbol{\varepsilon_r}$) of the measured samples is shown in Table 1 along with the bulk densities. For all specimens, the relative permittivity was nearly independent of frequency between 10 MHz and 3 GHz. The measured loss tangent was below the resolution of the measurement method (≤ 0.005), indicating very low dielectric losses.

16

The dependence of the relative permittivity on the sintering temperature followed the same trend as that of the bulk density [36]. The density increased with the sintering temperature, indicating that higher sintering temperatures led to lower porosity and more compact structures, which is consistent with the observed changes in the microstructures (see Figures 7 and 8).

Table 1 Final bulk densities (ρ) and relative permittivity

for sintered samples.

Sample	$\rho/\text{g·cm}^{-3}$	ε_r
AM–0–1200	1.75	2.91
AM–60–1200	1.83	3.28
AM–0–1300	1.61	3.21
AM–60–1300	1.90	3.53
AM–0–1400	2.08	3.49
AM–60–1400	2.22	4.04
AM–0–1500	2.86	4.41
AM–60–1500	2.71	4.69
AM–0–1600	3.26	6.15
AM–60–1600	3.21	5.65

This suggests that the higher density and more homogeneous microstructures were responsible for the higher dielectric permittivity obtained for increased sintering temperatures.

The permittivity increased more than 100 %, from as low as ~ 2.9 for AM–0–1200, to over 6 for AM–0–1600. Mechanically activated samples exhibit consistently higher values of the bulk density and permittivity at sintering temperatures below 1600 ℃, due to the smaller particle size and improved sintering caused by the mechanical activation [10].

Raman spectra of non-activated and mechanically activated samples, sintered in the range 1200–1600 ℃, are presented in Figure 10. $MgAl_2O_4$ belongs to the space group *Fd3m*, and exhibits five Raman active modes ($A_{1g}+E_g+3T_{2g}$) [37, 38]. All five Raman active modes were observed, and their positions and intensity ratios were in good agreement with literature data. In normal spinel, only two sharp and well-defined peaks were observed above 600 cm^{-1}, while for the inverse spinel, an additional A_{1g} peak appears at about 724 cm^{-1} [39, 40]. The presence of this additional A_{1g} peak was observed in all Raman spectra shown in Figure 10, indicating the degree of disorder. The lowest intensity of this peak is detected for AM–0–1200, and with increasing sintering temperature, the intensity of the peak increased, along with broadening of all observed peaks, suggesting an increase in the degree of disorder.
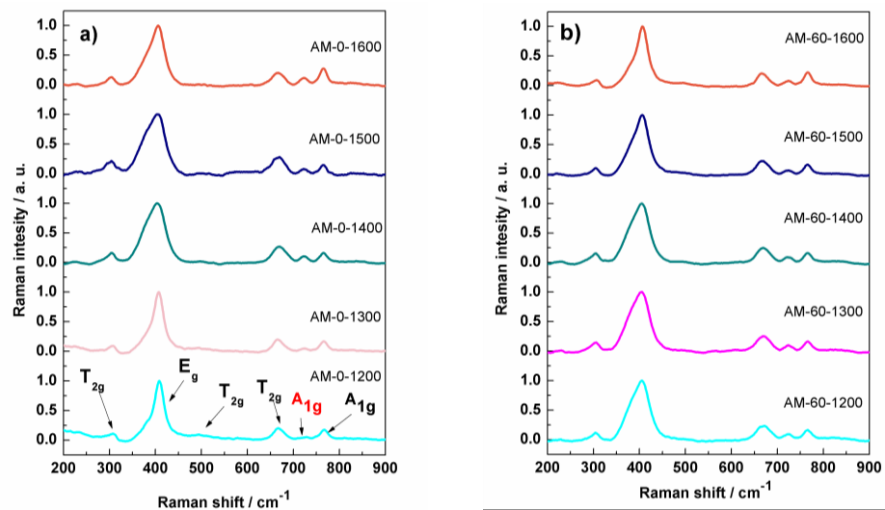
The effects of sintering temperature and mechanical activation on disorder were investigated in more detail by deconvoluting the Raman spectra. Peaks in the range 630–800 cm^{-1} were fit to individual Lorentzian peaks as shown in Figure 11. A previous study has shown that the mode at ~ 723 cm^{-1} has the same symmetry as the mode at ~ 770 cm^{-1} [24]. The peak at ~ 723 cm^{-1} has been identified as a breathing mode of AlO_4 tetrahedral, which is connected to the presence of cationic disorder.
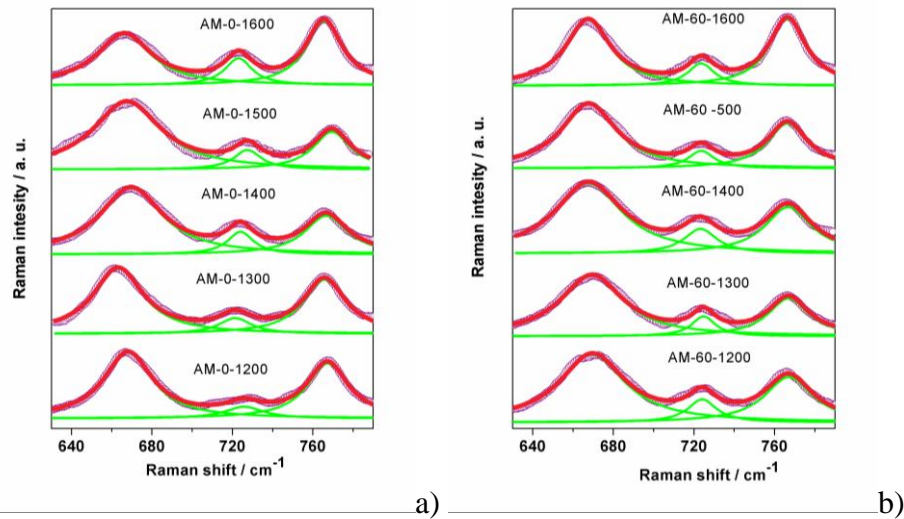
Figure 11 Deconvolution of Raman spectra of: a) non-activated and sintered samples and b) activated and sintered samples (green lines – separated Lorentzian peaks, red line – sum of Lorentzian peaks, blue circles – measured data).

In contrast, the peak at ~ 770 cm^{-1} has been identified as symmetric stretching of Mg–O bonds in MgO_4 tetrahedra, which is correlated to an ordered structure. Hence, the intensity

ratio of these separated Lorentzian peaks can be used as a measure of disorder in $MgAl_2O_4$. The intensity ratios of peaks at 723 and 770 cm^{-1}, for non-activated and activated samples vs. sintering temperature, is presented in Figure 12.
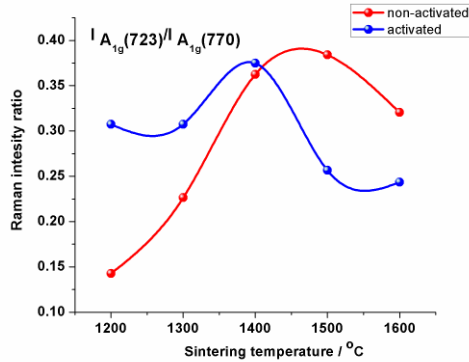
Figure 12 Intensity ratio of Lorentzian peaks at ~723 and ~770 cm^{-1} as a function of sintering temperature for non-activated and activated powders.

The level of disorder initially increased with increasing sintering temperature. As shown in Figure 12, the level of disorder increased up to 1500 ^{o}C for non-activated powders and 1400 ^{o}C for activated samples. The initial increase in disorder with increasing sintering temperature is consistent with previous reports while the decrease at higher temperatures is presumably due to annihilation of defects at higher temperatures. Comparing the non-activated and activated samples shows that mechanical activation leads to an increase in the degree of the exchange between Mg and Al cations, which may be due to the introduction of defects during the milling process.

In addition to the peak intensity ratios, disorder in spinel structure can be observed through changes in symmetry and width of E_g mode at ∼ 410 cm^{-1}, where the width of this mode increased due to an increase in inverse spinel content with increasing temperature [24, 37]. According to available literature data, all previous studies involving Raman measurements for $MgAl_2O_4$ spinel were performed for materials heat up to only 1400 °C [24, 37, 38]. The present study extends the investigation of the order-disorder ratio to samples sintered up to 1600 °C. Changes in width of E_g mode were fitted by a Lorenzian function, and the obtained results are presented in Figure 13. Changes in the full width at the half maximum (FWHM) of E_g peak followed same trend as the changes in the intensity ratio of Lorentzian peaks at ∼723 and ∼770 cm^{-1}. For non-activated samples, the breaking point for ordering of the crystal structure was around 1500 °C, while this point shifted to 1400 °C for activated samples, indicating that mechanical activation lowers the temperature of the ordering of the crystal lattice by about 100 °C.
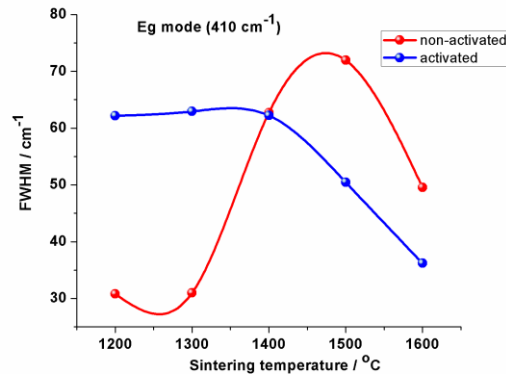

Figure 13 The FWHM values of the 410 cm^{-1} mode as a function of the sintering temperatures for non-activated and mechanically activated samples.

Conclusions

21

The influence of mechanical activation on microstructure, crystallization kinetics, and cation ordering in the $MgAl_2O_4$ spinel was investigated. The main conclusions are:

(1) 60 min of mechanical activation led to mechanochemical reaction within the initial powder; activation produced powders that appeared to be homogeneous with a reduction in agglomerate and particle size, compared to the non-activated powders.

(2) DTA indicated several processes took place during heating: loss of adsorbed water, decomposition of $Mg(OH)_2$, and decarbonization of MgO. In addition, an exothermic peak corresponding to the spinel formation was observed. This peak shifting from 1100–1400 ºC for non-activated powders to 950–1150 ºC after activation, with a corresponding reduction in value of E_a from 580 to 420 kJ·mol^{-1}.

(3) Analysis of microstructures showed that AM–0–1600 and AM–60–1600 had no open porosity, indicating that the final stage sintering was reached. As density increased, the pores became more regular in shape. The increased density also led to increases in the dielectric permittivity, from the lowest values of less than 3 after sintering at 1200 °C to values of more than 6 after sintering at 1600 °C. Furthermore, one phase system after sintering is obtained for all samples.

(4) Cation inversion was observed in all of sintered samples based additional Raman peak at 724 cm^{-1}. An increase in inversion was observed with increasing sintering temperature and the degree of inversion was higher in mechanically activated samples. Detailed analysis of Raman spectra indicated the breaking point for ordering of crystal structure to be around 1500 ºC for non-activated samples, while that point for activated samples is shifted to 1400 ºC.

(5) Finally, mechanical activation, as a preparation process, had a strong influence on all hierarchical levels within the powders and sintered samples: it affected the chemical

22

reaction, lowered the temperature of the spinel formation by about 200 ºC, and lowered the temperature of arrangement of the crystal lattice by about 100 ºC.

References

[1] Sadegh Abdi M, Ebadzadeh T, Ghaffari A, Feli M. Synthesis of nano-sized spinel ($MgAl_2O_4$) from short mechanochemically activated chloride precursor and its sintering behaviour, Adv Powd Technol. 2015;26:175–179.

[2] Quan Z, Wang Z, Wang X, Liu H, Ma Y. Effect of CeO_2 addition on the sintering behaviour of pre-synthesized magnesium aluminate spinel ceramic powders, Ceram Inter. 2019;45:488–493.

[3] Khorramirad M M, Rahimipour M R, Hadavi S M M, Shirvani Jozdani K. The effect of magnesium compounds (MgO and $MgAl_2O_4$) on the synthesis of Lanthanum magnesium hexaaluminate ($LaMgAl_{11}O_{19}$) by solid-state reaction method, Ceram Inter. 2018;44:4734–4739.

[4] Rahmat N, Yaakob Z, Pudukudy M, Abdul Rahman N, Suriani Jahaya S. Single step solid-state fusion for $MgAl_2O_4$ spinel synthesis and its influence on the structural and textural properties, Powd Technol. 2018;329:409–419.

23

[5] Raghu R, Nampoothiri J, Satish Kumar T. In-situ generation of $MgAl_2O_4$ particles in Al-Mg alloy using H_3BO_3 addition for grain refinement under ultrasonic treatment, Measur. 2018;129:389–394.

[6] Shahbazi H, Tataei M. A novel technique of gel-casting for producing dense ceramics of spinel ($MgAl_2O_4$), Ceram Inter. 2019;45:8727–8733.

[7] Bai J, Liu J, Li C, Li G, Du Q. Mixture of fuels approach for solution combustion synthesis of nanoscale $MgAl_2O_4$ powders, Adv Powd Technol. 2011;22:72–76.

[8] Saberi A, Golestani-Fard F, Sarpoolaky H, Willert-Porada M, Gerdes T, Simon R, Liebscher C. Development of $MgAl_2O_4$ spinel coating on graphite surface to improve its water-wettability and oxidation resistance, Ceram Inter. 2009;35:457–461.

[9] Ewais E M M, El-Amir A A M, Besisa D H A, Esmat M, Anadouli B E H. Synthesis of nanocrystalline $MgO/MgAl_2O_4$ spinel powders from industrial wastes, J All Comp. 2017;691:822–833.

[10] Obradović N, Fahrenholtz W G, Filipović S, Kosanović D, Dapčević A, Đorđević A, Balać I, Pavlović V B, The effect of mechanical activation on synthesis and properties of $MgAl_2O_4$ ceramics, Ceram Inter. 2019;45(9):12015–12021.

[11] Bar-On P, Lin I J, Nadiv S, Melamud M. Formation of partially inverse Mg−Al spinel by grinding MgO with γ-Al_2O_3, J Therm Anal Calorim. 1994;42(1):207–217.

[12] Filipović S, Obradović N, Pavlović V B, Marković S, Mitrić M, M. Ristić, M M. Influence of Mechanical Activation on Microstructure and Crystal Structure of Sintered MgO-TiO_2 System, Sci Sinter. 2010;42:143–151.

[13] Ristić M M, Milošević S Đ, Mechanical activation of inorganic materials, SASA Monographs 38, Beograd, 1998.

24

[14] Аввакумов Е Г. Механические методы активации хумических процессоб, Новосибирск: Изд-во Наука, Сибирское отд-ние, 1986.

[15] Filipović S, Obradović N, Marković S, Đorđević A, Balać I, Dapčević A, Rogan J, Pavlović P. Physical Properties of Sintered Alumina Doped with Different Oxides, Sci Sinter. 2018;50:409–419.

[16] Branković A. Mechanochemical Activation of $(SeO_2+Na_2CO_3)$ Mixture and Sodium Selenite Synthesis in Vibrational Mill, J Sol St Chem. 1998;135:256–259.

[17] Obradović N, Filipović S, Pavlović V, Mitrić M, Marković S, Mitić V, Đorđevic N, Ristic M M. Isothermal sintering of barium-zinc-titanate ceramics, Ceram Inter. 2011;37:21–27.

[18] Heinicke G. Tribochemistry, Academie-Verlag, Berlin, 1984.

[19] Obradović N, Gigov M, Đorđevic A, Kern F, Dmitrović S, Matović B, Đorđević A, Tshantshapanyan A, Vlahović B, Petrović P, Pavlović V. Shungite – a carbon-mineral rock material: Its sinterability and possible applications, Proc App Ceram. 2019;13(1):89–97

[20] Obradović N, Pavlović V, Kachlik M, Maca K, Olćan D, Đorđević A, Tshantshapanyan A, Vlahović B, Pavlović V. Processing and properties of dense cordierite ceramics obtained through solid-state reaction and pressure-less sintering, Adv Appl Ceram. 2018, DOI: 10.1080/17436753.2018.1548150

[21] Kostić E. Activation of solid state processes in Sintering and Materials, International Academic Publishers, Beijing, 1995;142–147.

[22] Pavlović M, Andrić Lj, Radulović D, Drmanić S, Đorđevic N, Petrov M. Influence of mechanical activation of a cordierite-based filler on sedimentation stability of lost foam refractory coatings, Sci Sinter. 2019;51:15–25.

25

[23] Ganesh I. A review on magnesium aluminate ($MgAl_2O_4$) spinel: synthesis, processing and applications, Inter Mater Rev. 2013;58(2):63–112.

[24] Muche D N F, Marple M A T, Hung I, Gan Z, Castro R HR, Sen S. Size-Induced Structural Disorder Enables Ultrahard Oxides, J Phys Chem C. 2017;121:13898−13905.

[25] Slotznick S P, Shim S H. In Situ Raman Spectroscopy Measurements of $MgAl_2O_4$ Spinel up to 1400 °C, Am. Mineral. 2008;93(2–3):470–476.

[26] Blagojević V. ThermV v0.2, https://sourceforge.net/projects/thermv/

[27] Chanda D Kr, Sekhar Das P, Samanta A, Dey A, Kumar Mandal A, Das Gupta K, Maity T, Kumar Mukhopadhyay A. Intertwined nanopetal assembly of $Mg(OH)_2$ powders, Ceram Inter. 2014;40:11411–11417.

[28] Obradović N, Terzić A, Pavlović Lj, Filipović S, Pavlović V. Dehydration investigations of a refractory concrete using DTA method, J Therm Anal Calorim. 2012;110:37–41.

[29] Fricker K J, Park A H. Effect of H_2O on $Mg(OH)_2$ carbonation pathways for combined CO_2 capture and storage, Chem Eng Sci. 2013;100:332–341.

[30] Li Z, Yu Q, Chen X, Liu H, Zhang J, Zhan J, Yang Y, Wei J. The role of MgO in the thermal behavior of MgO–silica fume pastes, J Therm Anal Calorim. 2017;127:1897–1909.

[31] Kissinger H E. Reaction kinetics in differential thermal analysis, Anal Chem. 1957;29:1702.

[32] Sinhamahapatra S, Shamim M, Tripathi H S, Ghosh A, Dana K. Kinetic modelling of solid state magnesium aluminate spinel formation and its validation, Ceram Inter. 2016;42:9204–9213.

[33] Ortega A. A simple and precise linear integral method for isoconversional data, Thermochim Acta, 2008;474:81.

[34] Vyazovkin S V, Lesnikovich A I. An approach to the solution of the inverse kinetic problem in the case of complex processes: Part 1. Methods employing a series of thermoanalytical curves, Thermochim Acta, 1990;165:273–280.

[35] Khawam A, Flanagan D R. J. Phys. Chem. B 2006;110:17315–17328.

[36] Obradović N, Filipović S, Đorđević N, Kosanović D, Pavlović V, Olćan D, Đorđević A, Kachlik M, Maca K. Microstructural and Electrical Properties of Cordierite-based Ceramics Obtained After Two-step Sintering Technique, Sci Sinter. 2016;48:157–165.

[37] Minh N V, Yang I-S. A Raman study of cation-disorder transition temperature of natural $MgAl_2O_4$ spinel, Vib Spectrosc. 2004;35(1):93–96.

[38] Evarestov R A, Platonenko A, Zhukovskii Y F. Site symmetry approach applied to the supercell model of $MgAl_2O_4$ spinel with oxygen interstitials: *Ab initio* calculations, Comput Mater Sci. 2018;150:517-523.

[39] O'Horo M P, Frisillo A L, White W B. Lattice vibrations of $MgAl_2O_4$ spinel, J Phys Chem Solids. 1973;34(1):23–28.

[40] Lazzeri M, Thibaudeau P. Ab initio Raman spectrum of the normal and disordered $MgAl_2O_4$ spinel, Phys Rev B. 2006;74(14):140301.

27

Figure 1 Scheme of normal and inverse spinel crystal struicture.

Figure 2 SEM micrographs of a) non-activated and b) 60 min activated powder.

Figure 3 DTA–TG results for non-activated samples with different heating rates.

Figure 4 DTA–TG results for activated samples with different heating rates.

Figure 5 Spinel formation peaks from DTA in non-activated (a) and activated (b) powders; Effective values of E_a (isoconversional Ortega method) for formation of spinel (c).

Figure 6 Comparison of experimental and simulated curves for non-activated (a–c) and activated (d–f) samples at different heating rates with presumed model D2.

Figure 7 SEM micrographs of fracture surfaces of specimens: a) AM–0–1200, b) AM–0–1300, c) AM–0–1400, d) AM–0–1500, and e) AM–0–1600.

Figure 8 SEM micrographs of fracture surfaces of sintered samples: a) AM–60–1200, b) AM–60–1300, c) AM–60–1400, d) AM–60–1500, and e) AM–60–1600.

Figure 9 XRD patterns of: a) non-activated powder (AM–0) and b) powder activated for 60 minutes (AM–60), after heating to various temperatures for 2 h in air [10].

Figure 10 Raman spectra of a) non-activated and b) activated samples sintered in the range 1200–1600 $^{\circ}$C.

Figure 11 Deconvolution of Raman spectra of a) non-activated and sintered samples and b) activated and sintered samples (green lines – separated Lorentzian peaks, red line – sum of Lorentzian peaks, blue circles – measured data).

Figure 12 Intensity ratio of Lorentzian peaks at ~723 and ~770 cm^{-1} as a function of sintering temperature for non-activated and activated powders.

Figure 13 The FWHM values of the 410 cm^{-1} mode as a function of the sintering temperatures for non-activated and mechanically activated samples.